DOI: 10.1002/ ((please add manuscript number))

ZnO nanorod arrays as electron injection layers for efficient organic light emitting diodes

*Jorge Costa Dantas Faria[1], Alasdair J. Campbell[1] and Martyn A. McLachlan[2]**

1 J. Costa Dantas Faria, Dr A. J. Campbell, Department of Physics & Centre for Plastic Electronics, Imperial College London, SW7 2AZ.

2 Dr M. A. McLachlan, Department of Materials & Centre for Plastic Electronics, Imperial College London, SW7 2AZ

Keywords: Organic Electronics, **(**Organic) Light-Emitting Diodes, Conjugated Polymers, Zinc Oxide, Nanorods

Nanostructured oxide arrays have received significant attention as charge injection and collection electrodes in numerous optoelectronic devices. Zinc oxide (ZnO) nanorods have received particular interest owing to the ease of fabrication using scalable, solution processes with a high degree of control of rod dimension and density. Here we implement vertical ZnO nanorods as electron injection layers in organic light emitting diodes (OLEDs) for display and lighting purposes. Implementing our nanorods into devices with an emissive polymer, poly(9,9-dioctyluorene-alt-benzothiadiazole) (F8BT) and poly(9,9-di-n-octylfluorene-alt-N-(4-butylphenyl)dipheny-lamine) (TFB) as an electron blocking layer, brightness and efficiencies up to 8600 cd/m^2 and 1.66 cd/A were achieved. We highlight simple solution processing methodologies combined with post-deposition thermal processing to achieve complete wetting of the nanorod arrays with the emissive polymer. The introduction of TFB to minimize charge leakage and non-radiative exciton decay results in dramatic increases to device yields and provides an insight into the operating mechanism of these devices. We demonstrate the detected emission originates from within the polymer layers with no evidence of ZnO band-

edge or defect emission. The work represents a significant development for the on-going implementation of ZnO nanorod arrays into efficient light emitting devices.

1. Introduction

The development and investigation of ZnO nanostructures for optoelectronic applications is extensive and well-documented, showcasing a variety of morphologies achievable across a wide range of deposition techniques[1–9]. Of particular interest for device applications is the growth of ZnO nanorod arrays (NRAs) from low temperature, aqueous deposition techniques[10] which, over the past decade, has seen morphological improvements in alignment and uniformity through the introduction of precursor ZnO seed layers[11], pH control of the growth environment[12,13], additive incorporation[14], as well as manipulation of growth variables including duration and temperature[15–18]. Efforts to implement nanorod arrays into bulk heterojunction hybrid organic-inorganic photovoltaics (hPV) have led to improved devices attributed to improvements in charge collection[19,20]. Consequently, much of the NRA design considerations and post-deposition treatments have been governed by their eventual incorporation into hPV devices[21–23]. In parallel there has been growing interest in incorporating nanostructured ZnO into light-emitting devices, particularly for UV emission by combining n-type ZnO NRAs with an inorganic p-type materials such as GaN[24,25], with recent reports of p-type organic materials being studied with the motivation of achieving all solution processed devices[26]. Despite promising initial results with emissive devices the inclusion of ZnO NRAs in light emitting diodes (LEDs) remains less developed than hPVs. For example Yang et al only recently first reported efficiencies for a UV-emitting diode based on a ZnO NRA/poly(3,4-ethylenedioxythiophene): polystyrene sulfonate (PEDOT:PSS) structure[27]– almost a decade after Könenkamp et al first

reported UV emission from a diode based on the same materials[28]. Reports of visible light emission from devices of ZnO NRAs and light-emitting polymers such as polyfluorene (PFO)[29] or poly(2-methoxy-5-(2-ethylhexyloxy)-1,4-phenylenevinylene) (MEH-PPV)[30], are given by only electroluminescent (EL) emission spectra[31–33]. Within these reports, white emission is achieved through combined emission from the light emitting polymer (LEP) together with various defect states present in the NRAs. However, and to the best of our knowledge, the metrics which would further support claims of the potential of these devices for lighting or display applications, such as the luminance (in terms of cd/m^2) and lighting efficiency parameters (in terms of cd/A and lm/W), have yet to be reported. Comparison between available reports is also complicated by the fact that few devices are grown as standard architectures, leading to different operating mechanisms being discussed between authors.

In this article, we report on a nanorod hybrid LED (NHyLED) device, where vertically-aligned ZnO NRAs act as an electron injection/transport layer infiltrated with the green emitting polymer poly(9,9-dioctyluorene-alt-benzothiadiazole) (F8BT) in an inverted, top-anode geometry similar to that reported for conventional hPV devices. Through the incorporation of a second polymer layer, poly(9,9-di-n-octylfluorene-alt-N-(4-butylphenyl)dipheny-lamine) (TFB), as an electron blocker we show that NR HyLEDs can exceed luminance values of 1000 cd/m^2 thus demonstrating quantitatively for the first time their potential for general lighting applications.

2. Results and Discussion

We present two device structures, one with and one without a TFB layer (herein referred to as Device A and Device B, respectively). The device structures are ITO/ZnO (130 nm)/ZnO NRA (750 nm)/F8BT (450 nm)/TFB (0 or 50 nm)/MoO_x (10

nm)/Au (80 nm), in which the layer thicknesses are indicated in parentheses. Both polymers were purchased from American Dye Source while chemicals involved in the NRA growth were purchased from Sigma Aldrich. All materials were used as received without further purification.

The NRAs were first deposited on clean glass substrates, following the procedure we have previously outlined[34]. To aid nucleation and vertical alignment a 130 nm ZnO seed layer was first cast onto the substrates using sol-gel precursors. The substrates were then suspended in a hydrothermal growth solution of equimolar zinc nitrate hexahydrate and hexamethylenetetramine (HMT), along with potassium chloride (KCl) and polyethyleneimine (PEI) as additives to ensure uniformity and vertical alignment of the rods. Scanning electron microscopy (SEM) images show a highly uniform array with rods approximately 750 nm in length aligned predominantly perpendicular to the substrate (figures 1a and b), with a distribution of diameters around 70 nm (figure 1c). X-ray diffraction (XRD) measurements show that the rods are highly crystalline and oriented along the *c*-axis (002) of the ZnO wurtzite structure (figure 1d).

F8BT was dissolved in toluene at a concentration of 30 mg/ml (yielding 450 nm films on a planar substrate) to ensure effective infiltration of the array whilst still leaving sufficient polymer to separate the tips of the array and the top anode for device fabrication. Cross-sectional SEM showed that the initial spin-coating of the polymer results in a thick overlayer on the rods with little infiltration (figure 2a). Smith *et al* have reported on having to cast F8BT from 10 mg/ml solutions four times via spin coating in order to create a layer thick enough to fully infiltrate their InGaN/GaN NRA[35], but few experimental details are given in this respect in other published NR

HyLED reports and complete infiltration is often presumed. There are extensive reports within hPV literature, however, that show the need for post-deposition thermal treatment to overcome wetting issues between the polymer and the NRA[20,36,37]. From differential scanning calorimetry (DSC) measurements (Supplementary Information figure S1), our F8BT has glass transition T_g and melting temperatures T_m of 130 °C and 260 °C, respectively, in line with that reported by others and with no obvious signs of thermal degradation over multiple measurement cycles[38]. Annealing the coated NRAs to temperatures slightly above T_g for 20 minutes results in some uptake into the NRAs, however complete infiltration can only be achieved by annealing above the T_m giving an intermixed ZnO NRA:F8BT layer of total thickness ~900 nm (figure 2b).

For device fabrication the ZnO, NRA and F8BT depositions were carried out on pre-cleaned glass/ITO substrates. Thermal evaporation of the MoO_x/Au anode contact onto the top F8BT surface device and device characterization was carried out as discussed in the Methods Section.

The effect of annealing the F8BT above T_m compared to a non-heated sample can be clearly observed on the *J-V* characteristics of the diodes fabricated (figure 2c). Clear diode behavior is observed in both cases with the ratio of forward/reverse currents at ±4 V being 2.60 and 20.3 for the as-cast and melt devices, respectively. Forward current density is almost 1000 times greater (at 10 V) in the heated devices as interfacial contact between the polymer and array is increased. Light emission was observed from the as-cast devices, but driving voltages significantly exceeding 20 V were required to record luminances of < 1 cd/m^2. Similarly, despite the large current flowing through the melt processed devices there was little light detected. Through repeat measurements we were able to record only one instance of strong EL with a

light turn-on voltage (V_L) of 3.2 V and a maximum luminance of 878 cd/m^2 at 28.8 V (figure 2d) and a low current efficiency of 0.047 cd/A. Nonetheless, these results are significant given the luminance values exceeded 100 cd/m^2, which is required for display purposes and approaching the general lighting requirement of 1000 cd/m^2.

In order to address the undesirably low efficiencies and improve the yield of functional devices, we consider the band energies of the materials studied (figure 3a). It has been reported that the F8BT/MoO_x interface allows for efficient Ohmic hole injection due to the deep work function of MoO_x which pins to the highest occupied molecular orbital (HOMO) at the interface with the organic layer[39,40]. However, there is a large ~0.7 eV energy barrier to electron injection between the ZnO conduction band (CB) and the F8BT lowest unoccupied molecular orbital (LUMO); it has been suggested that electron injection is achieved due to the potential drop across the oxide/polymer interface as holes accumulate on the polymer side[41]. This mechanism is likely to occur in NR HyLEDs, too, but it is also possible that given the large NRA:F8BT interface that the number of conduction pathways for charge carriers is increased considerably, hence facilitating the overall electron injection. Furthermore, both experimental and theoretical studies show that nanostructured surfaces lead to dramatic enhancements of the internal electric field with a corresponding decrease in the Schottky barrier height for charge injection[42,43]. An enhancement to the injection current by a factor of 35 was reported even for an injection-limited contact[42]. Once the onset of electron injection is reached, it is likely that the devices become flooded with negative charge carriers. With the reported LUMO of F8BT of ~3 eV[44] and the CB of MoO_x ~6.7 eV[45], a negative barrier ϕ_e to excess electrons exists and so for Device A these electrons will continue to flow out of the device rather than undergo exciton recombination and light emission. Indeed, preliminary results of electron-only

ITO/ZnO/ZnO NRA/F8BT/Ca/Al devices show current densities that are approximately twenty times greater than those containing a planar ZnO layer only (Supplementary Information figure S2). This can be addressed by introducing an electron blocking layer at the F8BT/MoO_x interface. TFB is often used in conjunction with F8BT, to act as an electron blocker and to prevent non-radiative exciton decay at contact interfaces due to the large LUMO offset Δ_{LUMO} of ~0.7 eV between the two polymers[46]. Recently we have outlined a methodology that allows TFB to be cast directly onto F8BT with no detectable dissolution of the F8BT[47]. To incorporate the TFB layer, devices were prepared as previously. Following deposition and processing of the F8BT the TFB was cast and dried at 120 °C for 20 minutes before contact evaporation to create an overall layer structure of ITO/ZnO/ZnO NRA/F8BT/TFB/MoO_x/Au (Device B), figure 3b. We confirm that the addition of TFB has not impacted the infiltration of F8BT as shown in figure 3c, which also shows all layers of the device in addition to the top electrode.

With the inclusion of TFB, device yield, luminance and efficiency all increase markedly, supporting the concept that this interlayer assists in limiting the leakage of electrons and/or non-radiative dissociation of excitons at the contact interface. The spread for the highest recorded performance metrics for a set of 23 devices is illustrated in the frequency diagrams of figures 4a-b. Of these devices, 87% recorded a maximum luminance exceeding 1000 cd/m^2 with 75% of the set between 1000-3000 cd/m^2. The brightest device had a maximum luminance of 8600 cd/m^2. Considering the current efficiency values, ~22% of devices exceed 1 cd/A with a maximum of 1.66 cd/A recorded. Most (56%) of the devices recorded values under 0.3 cd/A, although in comparison to the TFB free devices all but one pixel recorded higher current efficiencies, similar behavior was observed with respect to power

efficiency, with a maximum value of 0.26 lm/W measured in Device B. The observed spread in the recorded data may be attributed to variations in the NRA length and polymer thickness across the devices, while the modest efficiency values can be explained by considering typical Device B current-voltage-luminosity (*J-V-L)* characteristics, figure 4c. The rapid forward bias increase in current with voltage is accompanied by a slow increase in luminance, despite a low V_L of 4.8 V. Significant light emission (>100 cd/m^2) is only achieved at high voltages *i.e.* those exceeding 15 V. This is consistent with the high current densities, ~1000 mA/cm^2, needed to achieve maximum current efficiencies (figure 4c inset). The high current-to-light intensity and electrical-to-optical power ratios result in reduced lighting efficiencies. The incorporation of TFB has clearly had a significant impact in improving devices and overcoming some of the inherent limitations related to charge balance and non-radiative exciton dissociation mechanisms although it is apparent that there is scope to address this in the future.

Finally, we note the differences in electroluminescence of the Device B architecture (figure 4d) compared with that reported elsewhere for ZnO NRA HyLEDs, most notably the lack of an emission peak at ~380 nm associated with ZnO band-edge emission[29,30,48]. In NRA based devices this is usually the most intense emission peak with weak contributions, attributed to emission from defect states, also reported in the 500-600 nm range. If UV emission from our NRAs is occurring it would overlap with the high absorbance regions of F8BT and TFB (figure 4d inset). The lack of any observable UV emission evident, allows us to rule out contributions to the detected EL from ZnO band-edge and defect state emission, hence all detected EL is attributed to radiative exciton recombination within the F8BT layer. The emission of F8BT normally exhibits a single emission peak at 550 nm with a shoulder at ~580

nm[47]. It is likely that the three distinct peaks observed here at 550, 590 and 680 nm are interference fringes arising as a result of our inherently thick device structures and changes to the electroluminescence characteristics of emitters due to the variation in thickness of ZnO nanoparticle layers has been previously reported[49]. Transmission measurements, through a device stack (without the evaporated contacts), show clear Fabry-Perot interference fringes in the optically transparent region > 500 nm (Supplementary Information figure S3a). This is confirmed by repeat measurements of other devices (Supplementary Information figure S3b) which again show three distinct peaks, however at different wavelength and relative intensities which would arise due to slight thickness variations between devices. Based on these results, and combined with its transparency over the visible region as well as the ability to be grown into a variety of nanostructures, it is hoped that the ZnO NRA can be further tailored to improve the out-coupling of light from the emissive organic layers[50–52].

3. Conclusions

In summary, we demonstrate the successful fabrication of hybrid ZnO NRA/polymer LEDs confirming for the first time their potential for display and lighting purposes. We have compared our device characteristics to well-established metrics for lighting performance frequently cited in OLED and PLED literature, namely the luminance, and current and power efficiencies with the majority of devices tested exceeding the luminance requirement for general lighting. Though efficiency values are modest, ongoing optimization should show increases across all metrics as well as a reduction

in the spread of device performance. NRAs have been previously highlighted as structures that may improve charge carrier injection or improve light out-coupling when used as external light extraction layers[42,53,54]. Here, the incorporation of an internal NRA, which can simultaneously exploit these potential advantages is presented with our best devices achieving brightness and efficiencies of 8600 cd/m^2 and 1.66 cd/A. The potential for further improvements in hybrid light emitting diodes by incorporation ZnO NRAs is an elegant solution that opens a pathway to improved devices.

4. Experimental

Device Preparation and Characterisation: ITO-coated glass substrates (PsioTec, sheet resistance ~14 Ω/sq) were cleaned with successive 10 minute ultrasonications of acetone, isopropanol and deionized water, before undergoing a 10 minute UV/Ozone exposure. For the ZnO seed layer, a solgel consisting of 0.75 M zinc acetate dihydrate and 2-aminoethanol dissolved in 2-methoxyethanol was prepared and cast onto the cleaned ITO substrates via spin coating. Substrates would then be annealed for 10 minutes at 300 ˚C. This spin-anneal step would be repeated three times. The substrates would then undergo a final 450 ˚C anneal for 1 hour. Following this, the substrates were suspended in a solution of equimolar (50 mM) zinc nitrate hexahydrate and hexamethylenetetramine (HMT), 200 mM of potassium chloride (KCl) and 20 mM of polyethyleneimine (PEI). The reaction was allowed to proceed for 2 hours at 95 °C to reach the serried NR length. Completed substrates were dried and moved into a nitrogen glovebox (H_2O and O_2 < 0.01 ppm) for polymer deposition. F8BT (116 kg/mol, dispersity 3.4) in toluene was cast from 30 mg/ml solution at 2000 rpm for 40s and then annealed at 270 ˚C for 20 minutes before a slow cool of 5

˚C/min back to room temperature. For Device B substrates, TFB (80 kg/mol, dispersity 2.4) in cyclohexanone (10 mg/ml) was spin coated onto the top F8BT surface and the substrates were annealed for 20 minutes at 120 ˚C. Thermal evaporation of the top anode contact was carried out through a shadow mask at a base pressure of 1×10^{-6} mbar at rates of 0.1 and 0.5 Å/s for MoO_x and Au, respectively, producing six 0.45 cm^2 devices per substrate. Both polymers were purchased from American Dye Source, whereas all ZnO precursors were purchased from Sigma Aldrich. All materials were used without further purification.

Device Characterisation: Device testing was carried out under an inert atmosphere using a Keithley 236 Source Measure Unit and a Minolta luminance meter. EL was measured with an Ocean Optics S2000 Fibre Optic Spectrometer.

Materials Characterisation: SEM images were carried out on chromium-coated samples using a FEGSEM Leo 1525 microscope. Cross-sections of bare NRA substrates were achieved by scratching the surface with a diamond pen, whereas polymer-coated samples were first submerged into liquid nitrogen and then cleaved. The thicknesses of the polymer and ZnO seed layers were confirmed with the aid of a Dektak 150 surface profilometer. A Panalytical X'Pert Pro diffractometer was used for XRD measurements. Absorbance information of the F8BT, TFB and ZnO NRA layers was obtained using a Bentham single-beam UV-vis system. Finally, a Toledo DSC 1 was used to measure the thermal transitions of the F8BT using three heating and cooling scans between 50-300 ˚C at a constant scan rate of 10 ˚C/min.

Acknowledgements

J.C.D.F. is grateful for support through the EPSRC Centre for Doctoral Training in Plastic Electronics, EP/G037515/1. The authors thank Dr Jonathan Downing (NIST) for useful discussions.

References

[1] A. B. Djurišić, Y. H. Leung, *Small* **2006**, *2*, 944.

[2] Z. L. Wang, X. Y. Kong, Y. Ding, P. Gao, W. L. Hughes, R. Yang, Y. Zhang, *Adv. Funct. Mater.* **2004**, *14*, 943.

[3] A. A. Al-Tabbakh, M. A. More, D. S. Joag, N. S. Ramgir, I. S. Mulla, V. K. Pillai, *Appl. Phys. Lett.* **2007**, *90*, 162102.

[4] Y. H. Leung, A. Djurisic, W. Hchoy, M. Haixie, J. Gao, K. Waicheah, K. Yankittyman, W. Kinchan, *J. Cryst. Growth* **2005**, *274*, 430.

[5] H. Yan, R. He, J. Pham, P. Yang, *Adv. Mater.* **2003**, *15*, 402.

[6] Z. Wang, X. Qian, J. Yin, Z. Zhu, *Langmuir* **2004**, *20*, 3441.

[7] M. Willander, O. Nur, Q. X. Zhao, L. L. Yang, M. Lorenz, B. Q. Cao, J. Zúñiga Pérez, C. Czekalla, G. Zimmermann, M. Grundmann, a Bakin, a Behrends, M. Al-Suleiman, a El-Shaer, a Che Mofor, B. Postels, a Waag, N. Boukos, a Travlos, H. S. Kwack, J. Guinard, D. Le Si Dang, *Nanotechnology* **2009**, *20*, 332001.

[8] S. Xu, Z. L. Wang, *Nano Res.* **2011**, *4*, 1013.

[9] M. A. McLachlan, H. Rahman, B. Illy, D. W. McComb, M. P. Ryan, *Mater. Chem. Phys.* **2011**, *129*, 343.

[10] L. Vayssieres, *Adv. Mater.* **2003**, *15*, 464.

[11] L. E. Greene, M. Law, D. H. Tan, M. Montano, J. Goldberger, G. Somorjai, P. Yang, *Nano Lett.* **2005**, *5*, 1231.

[12] M. Ashfold, R. Doherty, N. Ndiforangwafor, D. Riley, Y. Sun, *Thin Solid Films* **2007**, *515*, 8679.

[13] S. Baruah, J. Dutta, *J. Cryst. Growth* **2009**, *311*, 2549.

[14] J. M. Downing, M. P. Ryan, M. A. McLachlan, *Thin Solid Films* **2013**, *539*, 18.

[15] M. Guo, P. Diao, S. Cai, *J. Solid State Chem.* **2005**, *178*, 1864.

[16] Y. I. Jeong, C. M. Shin, J. H. Heo, H. Ryu, W. J. Lee, J. H. Chang, C. S. Son, J. Yun, *Appl. Surf. Sci.* **2011**, *257*, 10358.

[17] T. Ma, M. Guo, M. Zhang, Y. Zhang, X. Wang, *Nanotechnology* **2007**, *18*, 035605.

[18] S. Xu, N. Adiga, S. Ba, T. Dasgupta, C. F. J. Wu, Z. L. Wang, *ACS Nano* **2009**, *3*, 1803.

[19] D. Olson, S. Shaheen, R. T. Collins, D. S. Ginley, *J. Phys. Chem. C* **2007**, *111*, 16670.

[20] L. Baeten, B. Conings, H.-G. Boyen, J. D'Haen, A. Hardy, M. D'Olieslaeger, J. V Manca, M. K. Van Bael, *Adv. Mater.* **2011**, *23*, 2802.

[21] B. Conings, L. Baeten, H.-G. Boyen, D. Spoltore, J. D'Haen, L. Grieten, P. Wagner, M. K. Van Bael, J. V. Manca, *J. Phys. Chem. C* **2011**, *115*, 16695.

[22] L. Baeten, B. Conings, J. D'Haen, C. De Dobbelaere, A. Hardy, J. V Manca, M. K. Van Bael, *ChemPhysChem* **2012**, *13*, 2777.

[23] J. Huang, Z. Yin, Q. Zheng, *Energy Environ. Sci.* **2011**, 3861.

[24] W. I. Park, G.-C. Yi, *Adv. Mater.* **2004**, *16*, 87.

[25] O. Lupan, T. Pauporté, B. Viana, *Adv. Mater.* **2010**, *22*, 3298.

[26] X. W. Sun, J. Z. Huang, J. X. Wang, Z. Xu, *Nano Lett.* **2008**, *8*, 1219.

[27] Q. Yang, Y. Liu, C. Pan, J. Chen, X. Wen, Z. L. Wang, *Nano Lett.* **2013**, *13*, 607.

[28] R. Könenkamp, R. C. Word, C. Schlegel, *Appl. Phys. Lett.* **2004**, *85*, 6004.

[29] C. Y. Lee, J. Y. Wang, Y. Chou, C. L. Cheng, C. H. Chao, S. C. Shiu, S. C. Hung, J. J. Chao, M. Y. Liu, W. F. Su, Y. F. Chen, C. F. Lin, *Nanotechnology* **2009**, *20*, 425202.

[30] S.-L. Zhao, P.-Z. Kan, Z. Xu, C. Kong, D.-W. Wang, Y. Yan, Y.-S. Wang, *Org. Electron.* **2010**, *11*, 789.

[31] Y. Zhang, L. Ge, M. Li, M. Yan, S. Ge, J. Yu, X. Song, B. Cao, *Chem. Commun.* **2014**, *50*, 1417.

[32] D.-W. Wang, S.-L. Zhao, Z. Xu, C. Kong, W. Gong, *Org. Electron.* **2011**, *12*, 92.

[33] L. Duan, P. Wang, F. Wei, W. Zhang, R. Yao, H. Xia, *Solid State Commun.* **2014**, *200*, 14.

[34] J. Downing, M. P. Ryan, N. Stingelin, M. A. McLachlan, *J. Photonics Energy* **2011**, *1*, 011117.

[35] R. Smith, B. Liu, J. Bai, T. Wang, *Nano Lett.* **2013**, *13*, 3042.

[36] P. Atienzar, T. Ishwara, B. N. Illy, M. P. Ryan, B. C. O'Regan, J. R. Durrant, J. Nelson, *J. Phys. Chem. Lett.* **2010**, *1*, 708.

[37] D. C. Olson, Y.-J. Lee, M. S. White, N. Kopidakis, S. E. Shaheen, D. S. Ginley, J. A. Voigt, J. W. P. Hsu, *J. Phys. Chem. C* **2007**, *111*, 16640.

[38] M. J. Banach, R. H. Friend, H. Sirringhaus, *Macromolecules* **2003**, *36*, 2838.

[39] Y. Nakayama, K. Morii, Y. Suzuki, H. Machida, S. Kera, N. Ueno, H. Kitagawa, Y. Noguchi, H. Ishii, *Adv. Funct. Mater.* **2009**, *19*, 3746.

[40] M. T. Greiner, M. G. Helander, W.-M. Tang, Z.-B. Wang, J. Qiu, Z.-H. Lu, *Nat. Mater.* **2012**, *11*, 76.

[41] H. J. Bolink, E. Coronado, D. Repetto, M. Sessolo, E. M. Barea, J. Bisquert, G. Garcia-Belmonte, J. Prochazka, L. Kavan, *Adv. Funct. Mater.* **2008**, *18*, 145.

[42] M. Fina, S. S. Mao, *J. Appl. Phys.* **2012**, *112*, 024512.

[43] Q. Zhao, H. Z. Zhang, Y. W. Zhu, S. Q. Feng, X. C. Sun, J. Xu, D. P. Yu, *Appl. Phys. Lett.* **2005**, *86*, 203115.

[44] J.-S. Kim, L. Lu, P. Sreearunothai, A. Seeley, K.-H. Yim, A. Petrozza, C. E. Murphy, D. Beljonne, J. Cornil, R. H. Friend, *J. Am. Chem. Soc.* **2008**, *130*, 13120.

[45] M. Kröger, S. Hamwi, J. Meyer, T. Riedl, W. Kowalsky, A. Kahn, *Appl. Phys. Lett.* **2009**, *95*, 123301.

[46] J.-S. Kim, R. H. Friend, I. Grizzi, J. H. Burroughes, *Appl. Phys. Lett.* **2005**, *87*, 023506.

[47] J. Costa Dantas Faria, A. J. Campbell, M. A. McLachlan, *Submitted J. Mat. Chem. C* 2015. TC-ART-01-2015-000263

[48] A. Nadarajah, R. C. Word, J. Meiss, R. Könenkamp, *Nano Lett.* **2008**, *8*, 534.

[49] H. Lee, I. Park, J. Kwak, D. Y. Yoon, C. Lee, *Appl. Phys. Lett.* **2010**, *96*, 153306.

[50] B. R. Lee, E. D. Jung, J. S. Park, Y. S. Nam, S. H. Min, B.-S. Kim, K.-M. Lee, J.-R. Jeong, R. H. Friend, J.-S. Kim, S. O. Kim, M. H. Song, *Nat. Commun.* **2014**, *5*, 4840.

[51] J. Zhong, H. Chen, G. Saraf, Y. Lu, C. K. Choi, J. J. Song, D. M. MacKie, H. Shen, *Appl. Phys. Lett.* **2007**, *90*, 2005.

[52] S. W. Liu, J. X. Wang, Y. Divayana, K. Dev, S. T. Tan, H. V. Demir, X. W. Sun, *Appl. Phys. Lett.* **2013**, *102*, 053305.

[53] K.-K. Kim, S. Lee, H. Kim, J.-C. Park, S.-N. Lee, Y. Park, S.-J. Park, S.-W. Kim, *Appl. Phys. Lett.* **2009**, *94*, 071118.

[54] S. J. An, J. H. Chae, G.-C. Yi, G. H. Park, *Appl. Phys. Lett.* **2008**, *92*, 121108.

Figure Captions

Figure 1: Characterization of ZnO NRAs. SEM images of (a) a top view of a NRA and (b) a cross-section of the NRA, dashed lines highlight seed layer at base of NRA of thickness ~ 130 nm, scale bar: 500 nm. (c) The distribution of the rod diameters as measured along the hexagonal axis of greatest extent. (d) X-ray diffraction patterns comparing the crystallinity of the ITO/ZnO seed layer to ITO/ZnO seed layer/NRA. Starred-peaks indicate features of the ITO substrate.

Figure 2: Assessment of polymer infiltration into NRAs. (a) SEM cross-section image of as-cast F8BT showing no infiltration into the NRA. Inset: Likewise, little infiltration was observed of T_g annealed polymer. (b) SEM cross-section image showing full infiltration once F8BT has been annealed above T_m leaving a ~150 nm of smooth F8BT on top of the array. Scale bars = 1 μm. (c) J-V characteristics of ITO/ZnO/ZnO NRA:F8BT/MoO_3/Au devices showing the significant increase in current density as F8BT penetrates the array following the annealing procedure. (d) J-V-L characteristic of the ITO/ZnO/ZnO NRA:F8BT/MoO_3/Au device (schematic shown inset) which exhibited strong light emission (filled squares represent the current density and open squares.

Figure 3: (a) Flat-band energy level diagram for all materials discussed in device fabrication. Relevant to Device A is the difference between the F8BT LUMO and the MoO_x CB, ϕ_e ,is highlighted. Relevant to Device B is the TFB layer (shown with a dotted outline) and the offset in LUMO energies between the two polymer layers, Δ_{LUMO}. (b) Device B schematic. (c) Cross section SEM of Device B highlighting the addition of the TFB layer with a separate cross-section showing the top MoO_x/Au anode contact displayed inset for clarity..

Figure 4: Electrical and optical characterization of ITO/ZnO/NRA:F8BT/TFB/MoO_3/Au devices. Frequency diagrams for a sample of 23 devices showing the maximum recorded (a) luminance and (b) current efficiencies with the power efficiency shown in inset. (c) J-V-L characteristics for a typical device with the variation of current and power efficiency values shown inset. Filled squares correspond to the left ordinate axes and open squares to the right axes. (d) Device EL spectra with absorbance data for the individual polymer layers as well as for the ZnO NRA shown inset.

Figure 1

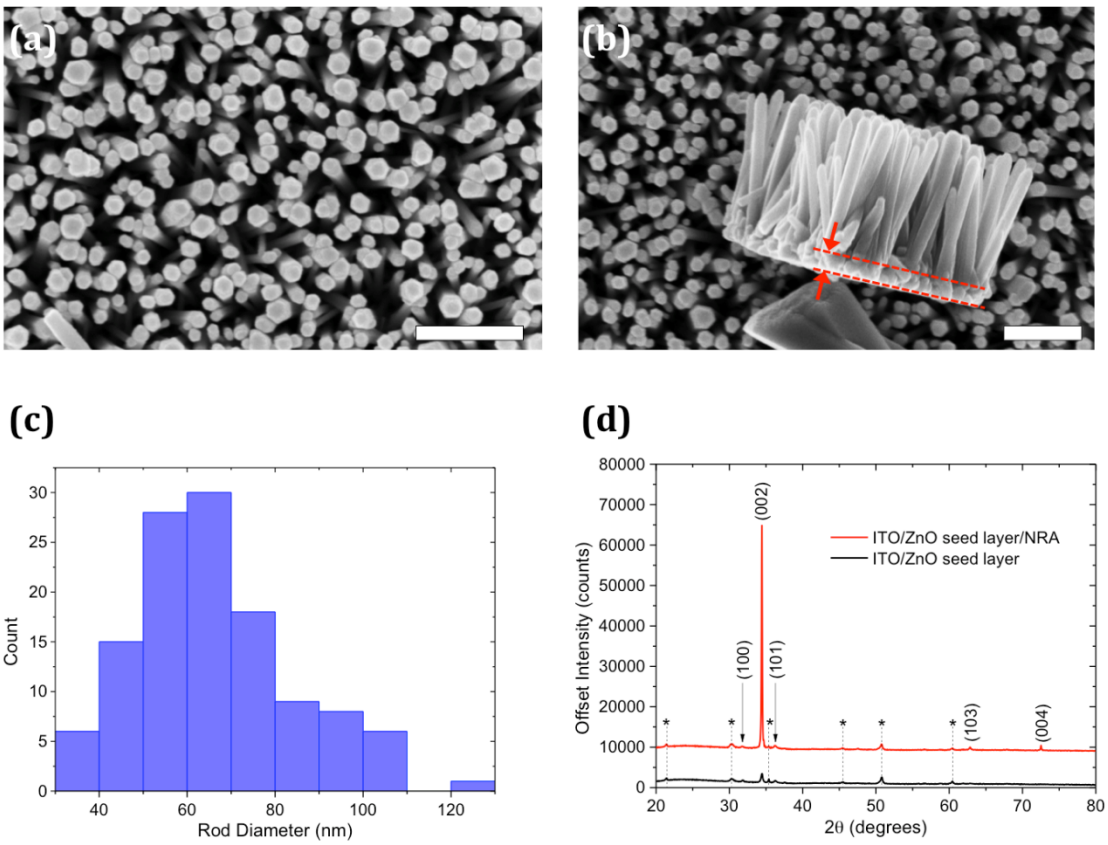
(a)
(b)
(c)
Count
Rod Diameter (nm)
(d)
Offset Intensity (counts)
2θ (degrees)
ITO/ZnO seed layer/NRA
ITO/ZnO seed layer
(002)
(100)
(101)
(103)
(004)

Figure 2:

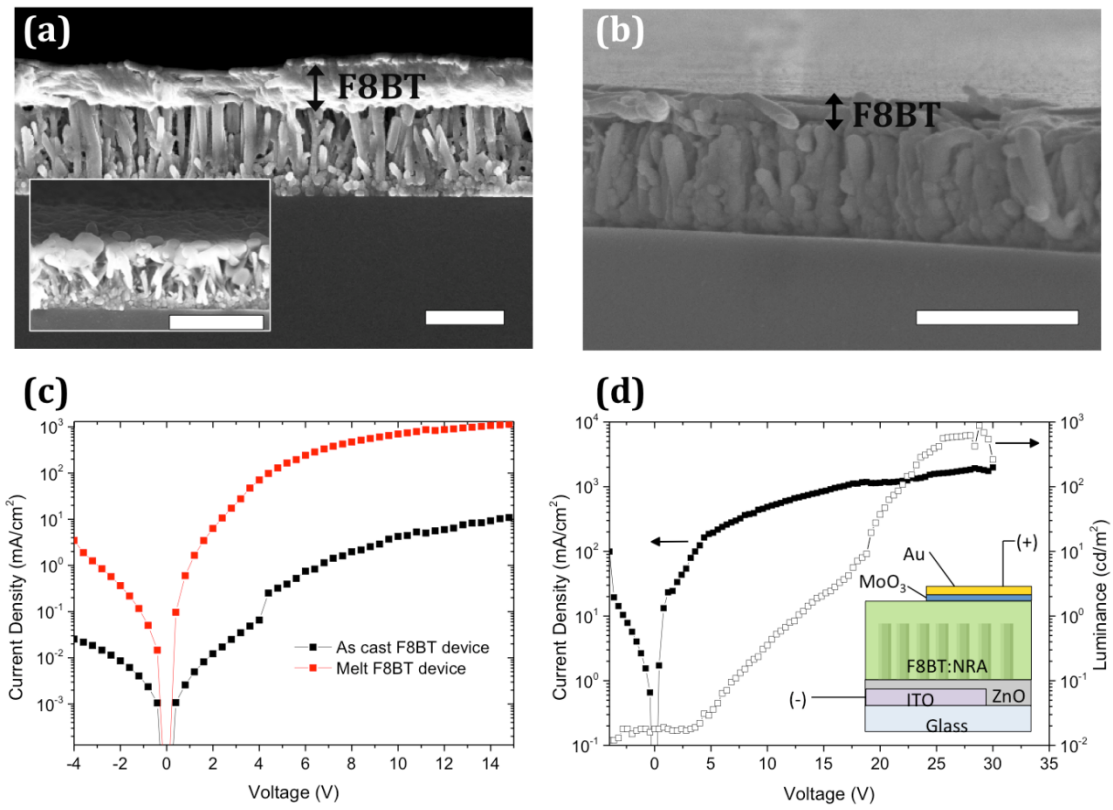
(a)
F8BT
(b)
F8BT
(c)
Current Density (mA/cm^2)
Voltage (V)
As cast F8BT device
Melt F8BT device
(d)
Current Density (mA/cm^2)
Luminance (cd/m^2)
Voltage (V)
Au
(+)
MoO_3
F8BT:NRA
(-)
ITO
ZnO
Glass

Figure 3:

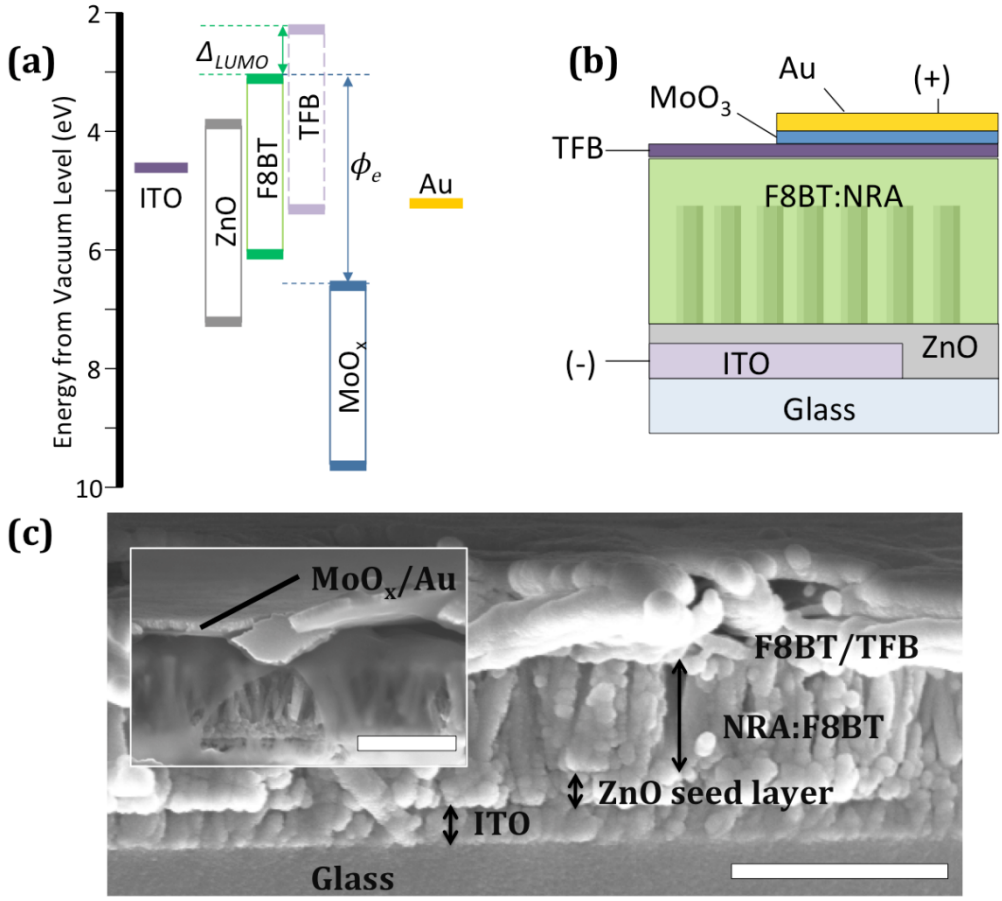
(a)
Energy from Vacuum Level (eV)
2
4
6
8
10
ITO
ZnO
F8BT
TFB
Δ_{LUMO}
ϕ_e
MoO_x
Au
(b)
Au
(+)
MoO_3
TFB
F8BT:NRA
ZnO
(-)
ITO
Glass
(c)
MoO_x/Au
F8BT/TFB
NRA:F8BT
ZnO seed layer
ITO
Glass

Figure 4:

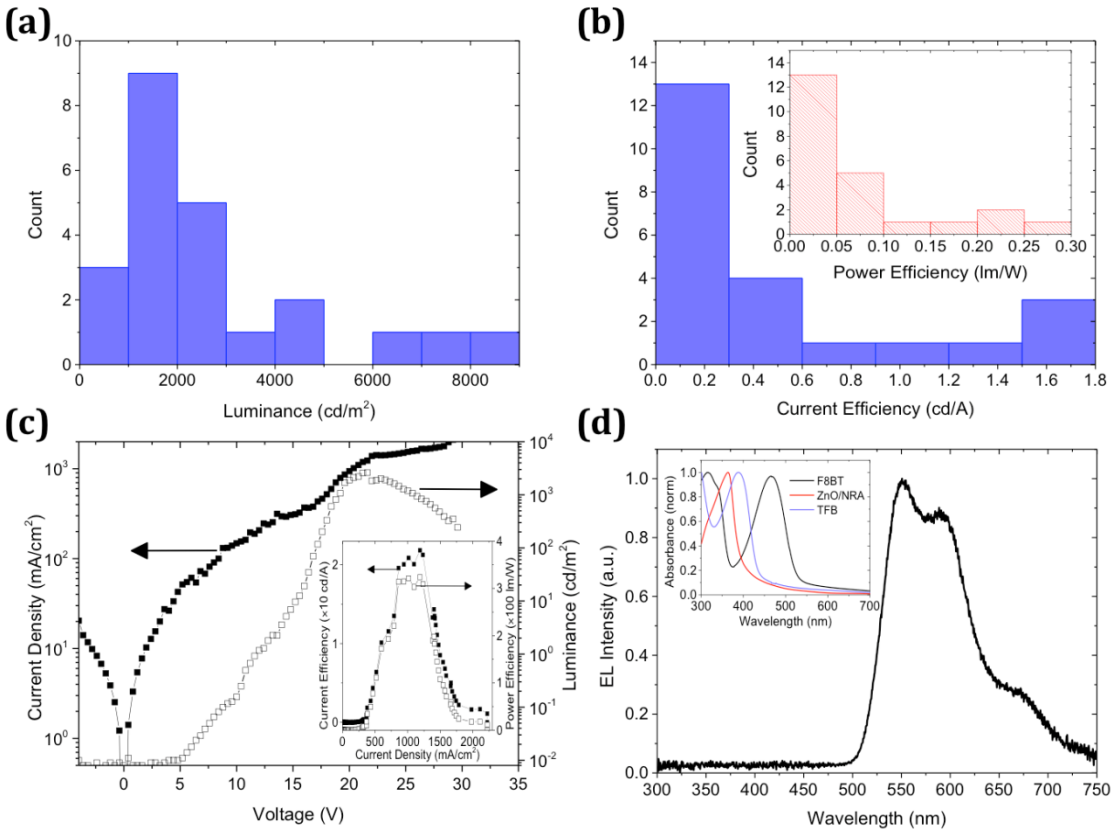
(a)
Count
Luminance (cd/m^2)
(b)
Count
Current Efficiency (cd/A)
Power Efficiency (lm/W)
(c)
Current Density (mA/cm^2)
Luminance (cd/m^2)
Voltage (V)
Current Efficiency (×10 cd/A)
Power Efficiency (×100 lm/W)
Current Density (mA/cm^2)
(d)
EL Intensity (a.u.)
Wavelength (nm)
Absorbance (norm)
F8BT
ZnO/NRA
TFB

Supporting Information

ZnO nanorod arrays as electron injection layers for efficient organic light emitting diodes

*Jorge Costa Dantas Faria, Alasdair J. Campbell and Martyn A. McLachlan**

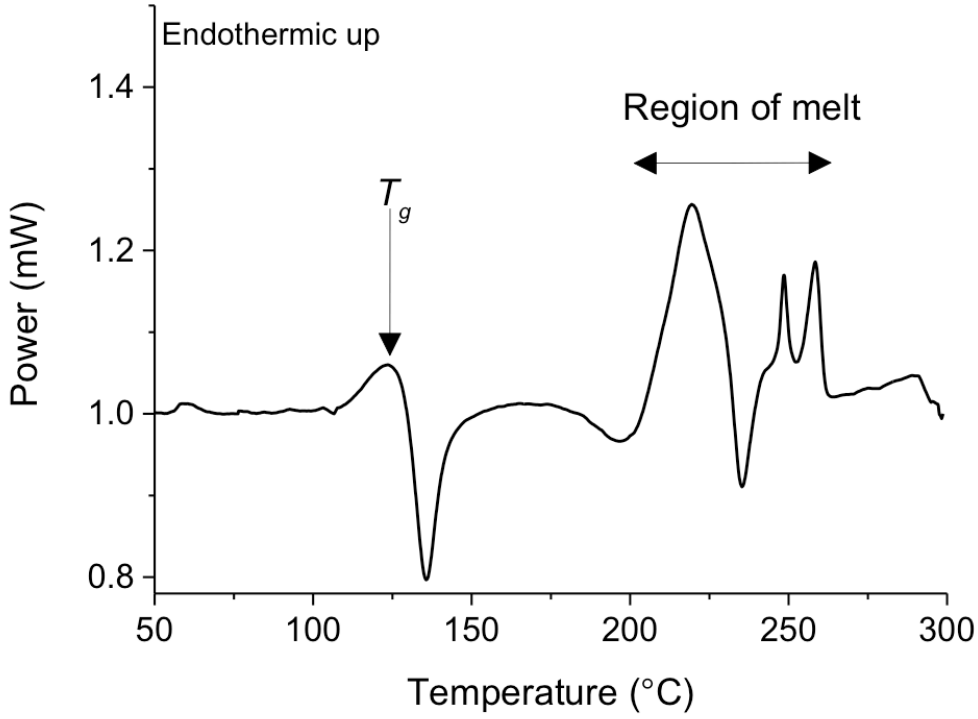

Figure S1: Differential scanning calorimetry (DSC) data for F8BT. The measurement was carried out using a Mettler Toledo DSC 1 using 3 mg of polymer with a heating and cooling rate of 10 K/min. The data shown is from the third heating cycle indicating good thermal stability. A glass transition peak is observed at 125 °C and immediately followed by a crystallization peak at 136 °C. Several endothermic peaks are observed between 200-260 °C, this is consistent with previous reports and is associated with the melting of different polymorphs.

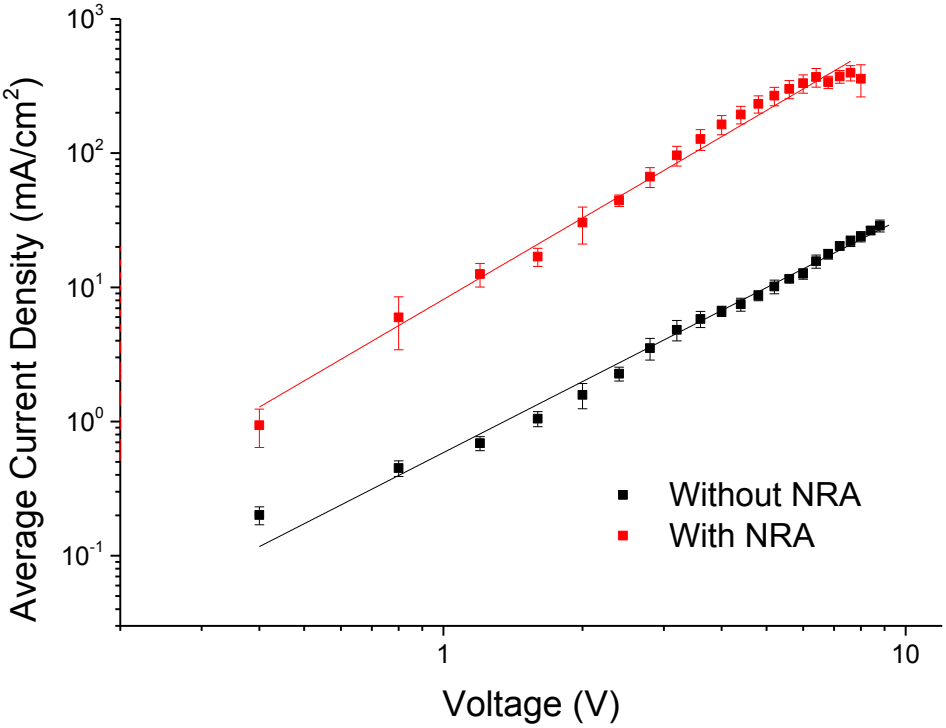

Figure S2: Electron-only devices with structure ITO/ZnO/F8BT/Ca/Al were compared with devices containing a ZnO NRA with structure ITO/ZnO/ZnO NRA/F8BT/Ca/Al. These results suggest that the NRA increases the electron current density by a factor of twenty compared to a planar ZnO layer.

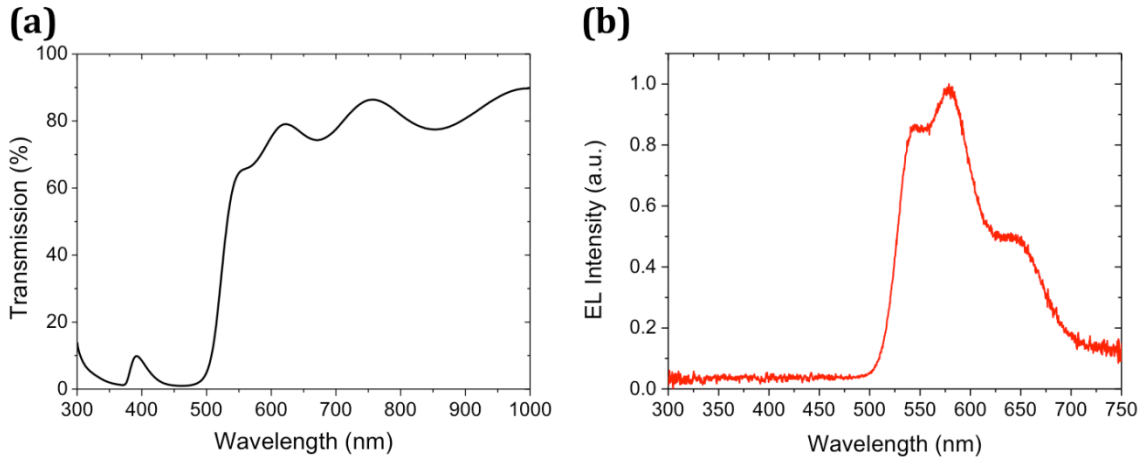

Figure S3: (a) Optical transmission spectra for a glass/ITO/ZnO/ZnO NRA:F8BT/TFB structure. Both TFB and ZnO absorptions contribute to the transmission minima at 370 nm while the minimum at 460 nm is due to absorption solely from the F8BT. Above 550 nm, clear interference fringes are observed highlighting the excellent uniformity of the device stack. (b) Another example of EL emission from Device B with different relative peak intensities and positions with respect to the EL shown in figure 4d.